AGU PUBLICATIONS

Earth's Future

RESEARCH ARTICLE
10.1002/2017EF000609

Statistical wave climate projections for coastal impact assessments

P. Camus[1], I. J. Losada[1], C. Izaguirre[1], A. Espejo[1], M. Menéndez[1], and J. Pérez[1]

[1] Environmental Hydraulics Institute "IH Cantabria", Universidad de Cantabria, Santander, Spain

Key Points:
- Statistical global multimodel wave climate projections under different representative concentration pathways
- The proposed global statistical downscaling framework allows an easy regional projection of wave climate
- Climate change coastal impact assessment based on downscaling impact indicators using the global statistical framework

Corresponding author:
Camus P., camusp@unican.es

Citation:
Camus, P., I. J., Losada, C., Izaguirre, A., Espejo, M., Menéndez, and J., Pérez (2017), Statistical wave climate projections for coastal impact assessments, *Earth's Future*, *5*, 918–933, doi:10.1002/2017EF000609

Received 5 MAY 2017
Accepted 4 AUG 2017
Accepted article online 9 AUG 2017
Published online 14 SEP 2017

Abstract Global multimodel wave climate projections are obtained at 1.0° × 1.0° scale from 30 Coupled Model Intercomparison Project Phase 5 (CMIP5) global circulation model (GCM) realizations. A semi-supervised weather-typing approach based on a characterization of the ocean wave generation areas and the historical wave information from the recent GOW2 database are used to train the statistical model. This framework is also applied to obtain high resolution projections of coastal wave climate and coastal impacts as port operability and coastal flooding. Regional projections are estimated using the collection of weather types at spacing of 1.0°. This assumption is feasible because the predictor is defined based on the wave generation area and the classification is guided by the local wave climate. The assessment of future changes in coastal impacts is based on direct downscaling of indicators defined by empirical formulations (total water level for coastal flooding and number of hours per year with overtopping for port operability). Global multimodel projections of the significant wave height and peak period are consistent with changes obtained in previous studies. Statistical confidence of expected changes is obtained due to the large number of GCMs to construct the ensemble. The proposed methodology is proved to be flexible to project wave climate at different spatial scales. Regional changes of additional variables as wave direction or other statistics can be estimated from the future empirical distribution with extreme values restricted to high percentiles (i.e., 95th, 99th percentiles). The statistical framework can also be applied to evaluate regional coastal impacts integrating changes in storminess and sea level rise.

1. Introduction

The interest in evaluating socioeconomic damages due to climate change impact in coastal areas has increased because they are the most heavily populated and developed land zones in the world. Climate change variations of sea level, wave conditions, storm surge (SS), and precipitation are the relevant environmental drivers that produce coastal physical impacts. Flooding and erosion are the main noticeable impacts which have associated other economic consequences due to failure and damage to marine infrastructure. The analysis of these impacts should address the underlying uncertainty, which is a key question of climate change assessments for decision-makers. Diversity of options is needed to be taken into account for making smart policies that allow for regular revisions [*Hallegatte and Mach*, 2016].

Widely varying approaches are used to tackle socioeconomic assessments of climate change, being determined by the spatial scale of the study (global, regional, local) and the information available. Regarding environmental drivers, most of the coastal impact assessments only analyze the effect of sea level rise (SLR) [e.g., *Hallegatte et al*., 2011, 2013; *Nicholls et al*., 2011; *Hinkel et al*., 2014; *Le Cozannet et al*., 2014; *Brown et al*., 2016] neglecting waves and SS although they are a key contributor to flooding and coastal erosion and they are affected by climate change. The difficulty of incorporating wave variations in the quantification of the climate change impact is determined by various factors: (1) downscaling techniques must be applied to obtain wave climate changes because wave information is not directly available from global circulation models (GCMs); (2) analysis of beach stability, sediment transport or wave set-up and runup component of sea level depends on multivariate wave information (i.e., significant wave height, wave period and wave direction); (3) accumulated uncertainty through each step from climate change scenarios, GCMs and regional climate models (RCMs) should be quantified; (4) the systematic biases of the GCMs and RCMs [*Wang et al*., 2014a, 2014b] hamper their use in impact studies; and (5) coastal impact process-based models require

hourly time series of the environmental drivers at local scale resolution. Therefore, the ideal framework to perform an impact assessment at local resolution to adopt effective adaptation strategies would imply nesting different models and statistical methods to transfer future climate information from GCMs to projected coastal impacts. This approach includes: dynamical downscaling (DD) of GCMs, statistical corrections of RCMs, coastal forcing models, local scale coastal impact models [*Ranasinghe*, 2016]. However, hundreds of different combinations of forcing variables should be simulated to account for the cascade of uncertainty making this multiscale modeling approach presently unaffordable.

Concerning the step of obtaining wave changes due to climate change, a dynamical or statistical downscaling (SD) approach can be adopted. The DD would be able to better reproduce the physical response to climate model projected surface winds; but the computational resources are usually the limiting factor for climate model experiments. On the other hand, statistical downscaling methods (SDMs) can provide a more robust multimodel projection ensemble because a large number of GCMs can be projected due to a significantly lower computational time. The best reproduced atmospheric variable by the GCMs can be selected as predictor (e.g., sea level pressure fields are better represented in climate models than surface winds [*Wang et al.,* 2014a, 2014b]) and the model variability biases can be diminished using standardized predictors. One of the main limitations of the SDMs is that they require predictor and predictand data for sufficiently long period to be used in the training process but it can be solved using reanalysis and/or hindcast data (they can be considered as quasi-observations if they are sufficiently validated with instrumental data). On the other hand, the spatial resolution and spatial representativeness of an SDM depend on the underlying observational data set used as a reference.

Dynamical projections are generated using GCMs or RCMs as forcing of the wave model at global or regional scale (e.g., in semi-enclosed seas such as the Mediterranean Sea, swell wave boundary conditions are not essential), without a common downscaling procedure to facilitate the intercomparison. For example, for the AR5 [*IPCC*, 2013] climate change scenarios, projections at a global scale have been obtained for the EC-Earth model [*Dobrynin et al*., 2012], for an ensemble of eight dynamical Coupled Model Intercomparison Project Phase 5 (CMIP5) GCMs [*Hemer et al*., 2013] or for a multimodel GCM ensemble of eight CMIP5 AOGCMs [*Shimura et al*., 2015]. At regional scale, projections in the Eastern North Pacific are simulated for four GCMs of CMIP5 at 0.25° [*Erikson et al*., 2015].

Statistical projections are usually based on multivariate regression models. Significant wave height has been predicted at 6-hourly resolution from sea level pressure fields (SLP) at a global scale [*Wang et al*., 2014a, 2014b] or at regional scale [*Casas-Prat et al*., 2014] or at seasonal to interannual time scale [*Martínez-Asensio et al*., 2016]. *Mori et al*. [2013] projected wave height using an empirical formula as a function of sea surface winds. Wave climate changes from multimodel ensemble over Europe are obtained using a statistical downscaling approach based on SLP weather types (WTs) and for an optimal ensemble of models selected according to a skill criteria [*Perez et al*., 2015].

Differences in the outputs of the dynamical simulations or SDMs determine the analysis that can be performed. Wave dynamical projections provides time series of different sea state parameters which allows the analysis of extreme values [*Mori et al*., 2010; *Semedo et al*., 2013] even of compound variables [i.e., Wave Energy Flux; *Mentaschi et al*., 2017]. Extreme statistics (maximum values) from the projected time series using regression models [*Casas-Prat et al*., 2014; *Wang et al.,* 2014a, 2014b] can be estimated but limited to significant wave height. Weather-typing downscaling method extends the analysis to more variables but restricts the projections of extreme climate to high percentiles [*Camus et al*., 2014].

Another simplification to reduce the computational effort to assess the climate change coastal impacts consists in using empirical formulations or indicators as an alternative solution to process based models. For example, climate change wave variations in coastal processes or port operability are assessed using empirical expressions and introducing wave changes as a percentage of increase/decrease from global projections [*Sierra and Casas-Prat*, 2014]. Coastal flooding can be analyzed through the proxy total water level (TWL) which accounts the astronomical tide (AT), the SS and the wave set-up referenced to mean sea level [*Rueda et al*., 2017]. Future changes in extremes sea levels along Europe's coast are quantified using a similar definition which considers these four significant components of flooding levels [*Vousdoukas et al*., 2017]. In that work, an extreme value statistical analysis is applied to hourly time series of dynamical multimodel projections of the SS, waves and tides combined with SLR. Future simulations of each main climatic driver

are required with the resulting computational effort. Statistical approaches open the practical alternative of the direct downscaling of the impact indicators which integrates the effects of various environmental drivers. The main advantage of this simply approach is that a single predictand (the coastal impact indicator) is downscaled. The problem of physical consistency among the variables individually downscaled is overcome [*Casanueva et al*., 2014]. Moreover, statistical downscaling reduces the climate bias using standardized predictors avoiding the correction of the bias of the dynamical projections before applying coastal forcing and coastal impact models. Besides, the effect of the SLR can easily be introduced to estimate changes due to the combination with storminess while most of the studies evaluate only coastal impacts due to SLR or waves independently [*Sierra et al*., 2015]. Nonlinear amplifications of coastal waves due to propagation over SLR-induced depth changes [*Arns et al*., 2017] are not modeled in this work.

In this work, a SDM is applied at a global scale based on a wave hindcast as the reference predictand information to obtain projections at different spatial scales and assess climate change impacts. Two indicators are considered to perform a regional evaluation of coastal impacts: TWL for coastal flooding and the number of hours per year with overtopping flow over a threshold as an indicator of port operability. These two indicators are selected because they are multivariable dependent and the influence of the SLR is introduced differently. TWL includes surface elevations due to SS and AT, besides waves. Therefore, historical databases of AT and SS are needed to calibrate the statistical relationship between weather conditions and indicators of coastal impacts. Regional projections of SLR are also required to introduce the effect of the change in mean sea level.

The databases used are described in Section 2. The statistical approach for downscaling wave climate is detailed in Section 3, including a characterization of wave generation areas, model validation and verification of projected GCM climatology. Section 4 shows the multimodel ensemble global projections. Section 5 extends the applicability of the statistical downscaling framework to obtain regional wave climate projections along two coastal regions. Section 6 shows a regional assessment of coastal climate change impacts by means of direct downscaling of coastal indicators. Section 7 contains the conclusions.

2. Databases

2.1. Historical Data

2.1.1. Historical Atmospheric Data

The global SLP fields of the Climate Forecast System Reanalysis (CFSR and CFSRv2 [*Saha et al*., 2014]) are used to define the predictor of the statistical model. The temporal coverage spans from 1979 to 2015 with hourly temporal resolution and 0.5° spatial resolution.

2.1.2. Historical Wave Data

The wave hindcast developed by *Perez et al*. [2017] provides historical wave data (significant wave height, H_s, peak wave period, T_m, mean wave direction, θ_m) with hourly resolution and 0.5° spatial resolution at a global scale and 0.25° in the continental shelf along worldwide coast from 1979 onwards. This hindcast uses WaveWatch III wave model (version 4.18 [*Tolman*, 2014]) in a multigrid configuration. Winds and ice coverage were interpolated from CFSR and CFSv2 data.

2.1.3. Historical Sea Level Data

6-Hourly surge data from September 1992 to present on a regular grid of 0.25° × 0.25° corresponds to the dynamic atmospheric correction (DAC), produced by CLS Space Oceanography Division using the MOG2D model [*Carrère and Lyard*, 2003] from Legos and distributed by AVISO, with support from CNES (http://www.aviso.altimetry.fr/).

Hourly AT is reconstructed at 0.25° spatial resolution, using harmonic analysis from the outcomes of the global model of ocean tides (TPXO7.2) that assimilates data from TOPEX/Poseidon missions and tidal gauges for the common period of the other marine hazards.

2.2. Climate Model Projections

Daily SLP fields from the GCMs of the CMIP5 are used to obtain changes in the predictor. Data from historical climate experiments from 1975 to 2004 were used to characterize recent past conditions. Data from representative concentration pathways (RCPs) from 2070 to 2100 were used to represent long-term future

Table 1. CMIP5 GCMs (Names, Institutions, Atmospheric Resolutions) Used in Wave Projections

Model	Institution	Atmospheric Resolution (Lat. × Lon., Number of Layers)
ACCESS1.0	CSIRO-BOM (Australia)	1.25° × 1.9°, L38
ACCESS1.3	CSIRO-BOM (Australia)	1.25° × 1.9°, L38
BCC-CSM1.1	Beijing Climate Center (China)	2.8° × 2.8°, L26
BCC-CSM1.1(m)	Beijing Climate Center (China)	1.12° × 1.12°, L26
BNU-ESM	College of Global Change and Earth System Science (China)	2.8° × 2.8°, L26
CanESM2	Canadian Centre for Climate Modeling and Analysis (Canada)	2.8° × 2.8°, L35
CCSM4	National Center for Atmospheric Research (USA)	0.94° × 1.25°, L26
CESM1 (BGC)	Community Earth System Model Contributors (USA)	0.94° × 1.25°, L26
CESM1 (CAM5)	Community Earth System Model Contributors (USA)	0.94° × 1.25°, L26
CMCC-CM	Centro Euro-Mediterraneo per I Cambiamenti Climatici (Italy)	0.75° × 0.75°, L31
CMCC-CMS	Centro Euro-Mediterraneo per I Cambiamenti Climatici (Italy)	1.9° × 1.9°, L95
CNRM-CM5	Centre National de Recherches Météorologiques (France)	1.4° × 1.4°, L31
CSIRO-Mk3.6.0	CSIRO-QCCCE (Australia)	1.9° × 1.9°, L18
FGOALS-g2	LASG-CESS (China)	2.8° × 2.8°, L26
GFDL-CM3	NOAA Geophysical Fluid Dynamics Laboratory (USA)	2° × 2.5°, L48
GFDL-ESM2G	NOAA Geophysical Fluid Dynamics Laboratory (USA)	2° × 2.5°, L48
GFDL-ESM2M	NOAA Geophysical Fluid Dynamics Laboratory (USA)	2° × 2.5°, L48
HadGEM2-CC	Met Office Hadley Centre (UK)	1.25° × 1.9°, L60
HadGEM2-ES	Met Office Hadley Centre (UK)	1.25° × 1.9°, L38
INM-CM4	Institute for Numerical Mathematics	1.5° × 2°, L21
IPSL-CM5A-LR	Institut Pierre-Simon Laplace (France)	1.9° × 3.75°, L39
IPSL-CM5A-MR	Institut Pierre-Simon Laplace (France)	1.25° × 2.5°, L39
IPSL-CM5B-LR	Institut Pierre-Simon Laplace (France)	1.9° × 3.75°, L39
MIROC-ESM	MIROC (Japan)	2.8° × 2.8°, L80
MIROC-ESM-CHEM	MIROC (Japan)	2.8° × 2.8°, L80
MIROC5	MIROC (Japan)	1.4° × 1.4°, L40
MPI-ESM-LR	Max-Planck-Institut für Meteorologie (Germany)	1.9° × 1.9°, L47
MPI-ESM-MR	Max-Planck-Institut für Meteorologie (Germany)	1.9° × 1.9°, L95
MRI-CGCM3	Meteorological Research Institute (Japan)	1.1° × 1.1°, L48
NorESM1-M	Norwegian Climate Centre (Norway)	1.9° × 2.5°, L26

conditions. The RCP4.5 and RCP8.5 are selected as representative of a medium stabilization scenario and a very high baseline emission scenario, respectively. A total of 30 GCMs (see Table 1) with historical and RCP4.5 and RCP8.5 simulations are considered in this study. The CMIP5 data used in this study were obtained via the Earth System Grid—Center for Enabling Technologies (ESG-CET; http://pcmdi9.llnl.gov/).

The regional SLR by 2100 for RCP4.5 or RCP8.5 scenarios is extracted from the global projections of regional mean sea level obtained by *Slangen et al*. [2014] using a dynamical modeling that incorporates regional contributions of land ice, groundwater depletion and glacial isostatic adjustment, including gravitational effects due to mass redistribution. Results are provided for RCP4.5 and RCP8.5 for the end of the 21st century.

3. Statistical Downscaling Approach

3.1. Overall Methodology

A weather-typing approach is applied to project the global wave climate and to assess coastal impacts from future changes in the sea level pressure (SLP) fields [*Camus et al*., 2014]. A regression guided classification is applied to a combination of the weighted predictor and predictand estimations from a regression model linking the SLP fields with local marine climate. The level of influence of the wave data is controlled by

a simple weighting factor which balances the loss/gain of predictor/predictand representativeness [*Cannon*, 2012]. A factor equal to 0.6 is implemented globally based on a sensitivity analysis of the influence of the guided classification in the dispersion of the multivariate wave climate within WTs and the skill of the statistical approach in the North Atlantic Ocean [*Camus et al*., 2016].

Figure 1 shows the scheme of the statistical framework proposed to downscale wave climate at global and regional scale and to perform a regional climate change assessment by means of a direct downscaling of coastal impact indicators.

1. The global ocean is divided in 11 subdomains with a common predictor (spatial domain and historical temporal coverage) based on a global wave genesis characterization.
2. Wave data at spatial resolution of 1.0° obtained from GOW2 is used as reference predictand observations to establish the statistical relationship. A particular regression-guided classification is performed for each wave grid node taking into account multivariate wave conditions (H_s, T_p, θ) as predictand.
3. The mean value of each wave variable (e.g., H_s or T_p) is calculated for each WT at each wave grid node.
4. The global wave projections are estimated from the future probability of WTs and the mean value of the wave variables associated with each WT at each wave grid node.
5. The empirical distribution of hourly wave parameters at each grid node of the GOW2 wave database at regional scale (0.25°) for each WT corresponding to the closest global wave grid node (resolution 1.0° × 1.0°) is calculated. The same procedure is applied for the coastal impact indicators at regional scale (i.e., TWL for coastal flooding and the number of hours per year with overtopping flow over a threshold for port operability).
6. The future empirical distribution of the regional wave variables and the coastal impact indicators is obtained for each regional grid node using the future probability of WTs. The changes in regional wave parameters or impact indicators are estimated for 2010–2100 under RCP4.5 and RCP8.5.

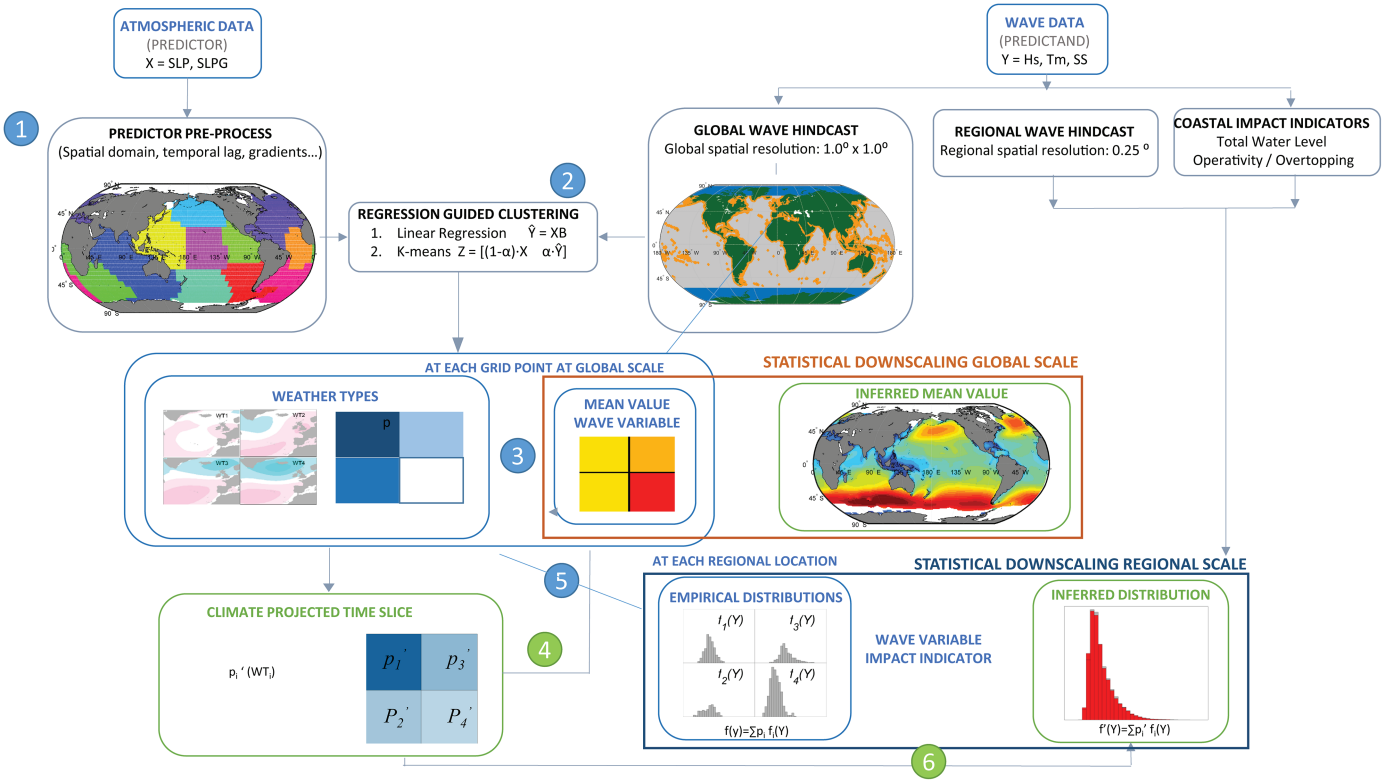

Figure 1. Scheme of the statistical downscaling methodology to obtain wave climate projections for coastal impact assessments. Steps in blue represent the fitting of the statistical model. Steps in green correspond to the processes to estimate climate changes in waves and coastal indicators. Global and regional scales of the methodology are differentiated depending on the statistical approach based on the mean value or the empirical distribution associated with each WT.

3.2. Characterization of Wave Genesis

The predictor for each location must represent the wind conditions that generate waves at that target location. Therefore, the spatial domain should cover the generation area for that particular location. Due to the global scale of this study, the ocean is divided in homogenous regions based on similar wave genesis. The Evaluation of Source and Travel-time of wave Energy reaching a Local Area (ESTELA) method [*Perez et al*., 2014] is used to distinguish these subdomains. ESTELAs are calculated each 5.0° from spectral information. ESTELA maps with high percentage of wave energy blocked by land (geographically based criteria) are not considered because they represent local conditions for a global classification. Many filters are applied to these maps in order to eliminate parts of the generation areas that are not relevant (i.e., travel time higher than 10 days, energy threshold). ESTELA data are transformed to values 1 and 0 (wave energy/not wave energy) to make the wave generation areas comparable within each map and between different maps. These data are classified using *K*-means algorithm (KMA), obtaining 11 wave generation patterns, shown in Figure 2. The subdomains are defined as the locations with the same pattern, represented at the same color as the corresponding pattern in Figure 2. The predictor spatial domain for each subdomain covers the wave generation pattern and the locations within this subdomain (marked by a black box in each pattern). It can observed how the wave origin in some areas come from both hemispheres. The mean travel time for each wave generation pattern defines the recent history of SLP conditions (predictor temporal coverage), varying from 7 days (subdomain 10) to 3 days (subdomain 7). The predictor is defined as the m-daily mean SLP and m-daily mean SLPG (squared SLP gradients), with *m* being a value from 3 to 7, depending on the subdomain, calculated every day through the historical time period [see *Camus et al*., 2014 for a more detail explanation of the predictor definition]. CFSR SLP data and CMIP5 SLP data are converted to a common 2.0°×2.0° latitude–longitude grid. Daily predictor fields are standardized to avoid biased results due to different scales. In the case of GCMs, standardization is applied using the simulated climatological mean and standard deviation for the historical period (1997–2005) which also diminishes the climate model biases.

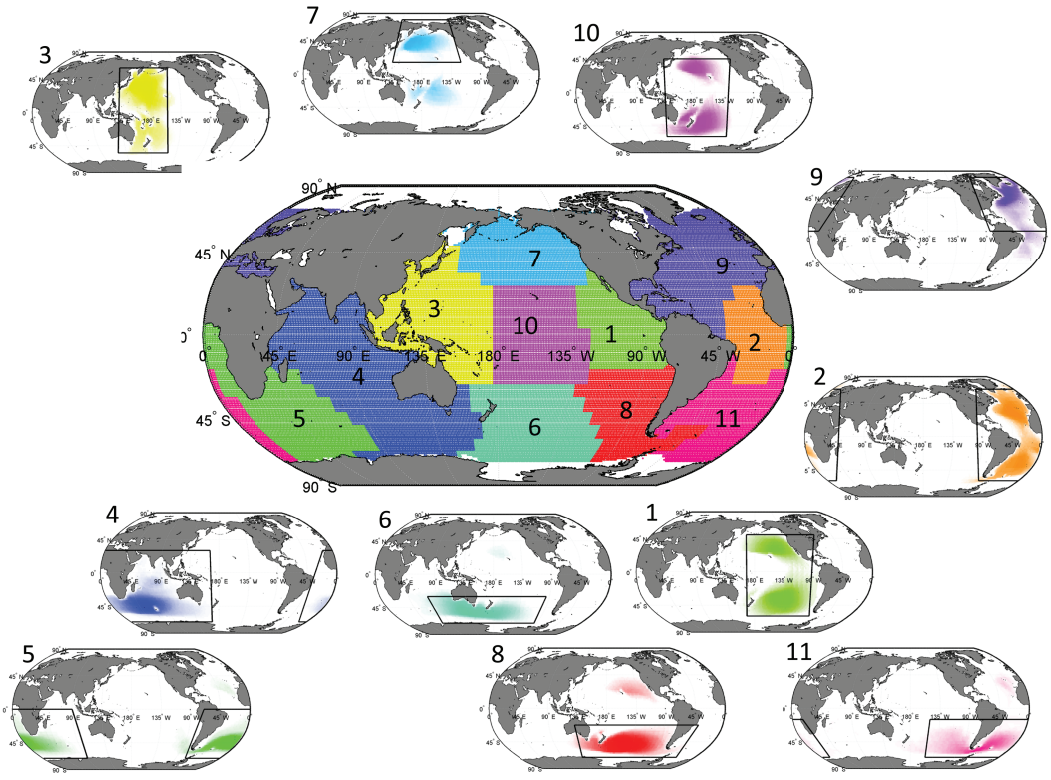

Figure 2. Wave subdomains based on 11 patterns of the wave generation areas. The subdomains are represented at the same color as the corresponding pattern. The predictor spatial domain for each subdomain is marked by a black box in each wave generation pattern.

3.3. Validation of the Statistical Downscaling Model

CFSR and GOW2 data from 1979 to 2015 are used in the training process, splitting them into a calibration period (1979–2005) and validation period (2006–2015). The probability of WTs is calculated in the validation period to infer the monthly local marine climate parameters. The model is validated by comparing the estimations of the monthly parameters calculated using the SDM and from the original time series of the wave hindcast database. The Pearson correlation coefficient (ρ) and the normalized root mean square error (*nrmse*, expressed in %) of the monthly mean significant wave height and mean period are calculated. Correlation for monthly H_s is between 0.85 and 0.98 while *nrmse* is around 4%–18%, being around 6% in 90% of the global ocean, limited to 18% in Indonesia, around 12% in the Gulf of Mexico and Mediterranean Sea and coastal areas of the Indian Sea and the North West Pacific. Regarding T_p, correlation decreases to values of 0.6 for the East Tropical Pacific, with maximum values of 0.92 for the North Atlantic Ocean. The *nrmse* is around 7% in most areas of the global ocean, with worse results in the area of Indonesia (values around 11%). Wave height changes will be expected to be estimated with higher confidence because the model has slightly higher skill for wave height than for peak period, which seems more difficult to be modeled.

3.4. Verification of the Projected GCM Climatology

Although the statistical downscaling approach reduces the climate model biases, the model's ability to reproduce the observed climate is verified in order to analyze if the uncertainty of each particular GCM projection can determine the ensemble future changes.

The multimodel mean bias of annual mean H_s, defined as the difference between the CMIP5-Ensemble and the GOW2-CFS climatology in the historical period 1979–2005, is lower than 0.15 m. A smaller H_s bias is reproduced in the Southern Ocean and Indian Ocean while higher values are obtained in the North Atlantic and the Pacific Ocean due to the more pronounced seasonal variability in the northern basins. *Hemer and Trenham* [2016] found a negative bias across the entire global ocean due to an expected reduced intensity of storm systems within the CMIP5 models. This underestimation of the storm intensity seems to be partially corrected using standardized predictors in the SDM. The multimodel mean bias of the absolute seasonality (JFM minus JAS) of monthly mean H_s is around 0.6 m, indicating an underestimation across the center of the northern Pacific and Atlantic Ocean (associated with underestimation of the JFM H_s) and across the Indian Ocean (associated with underestimation of the JAS H_s).

The performance of each particular GCM considered in this work is analyzed by comparing the GCM projections with the GOW2 dataset in a common period (1979–2005). Seasonal climatologies of H_s and T_p are compared using Taylor diagrams [*Taylor*, 2001]. Figure 3 shows the Taylor diagrams for the JFM and JAS spatial patterns of H_s and T_p for each GCM and the ensemble projections. This diagram synthesizes three standard metrics of spatial similarity — standard deviation, centered root-mean-square difference and correlation — in a single bidimensional plot. The standard deviations and the root-mean-square differences of each spatial pattern forced by each GCM are normalized dividing by the standard deviation of the observations. Besides, the color of each point indicates the spatially averaged mean absolute error (MAE), in order to avoid the compensation of opposite sign biases [*Casanueva et al*., 2016]. Better performance models are close to observation, on the *x*-axis (labeled as OBS in the figures). The climate bias and climate variability of each GCM are confirmed to be reduced in Figure 3. The verification scores are closer to observations at seasonal scale, the performance in JAS being worse (it can be observed in MAE) due to a slight underestimation of H_s across the Indian Ocean. Nevertheless, the statistical downscaling model reproduces reasonably well the climate for the seasonal cycle of H_s and T_p.

4. Global Wave Projections

Figure 4 shows the 30-model ensemble mean projected changes in annual and seasonal (JFM, JAS) H_s for the period 2070–2100 relative to the period 1979–2005 for the RCP8.5 scenario. The changes are considered consistent when the multimodel ensemble mean variation exceeds the intermodel standard deviation and if more than 80% of the significant models agree on the sign. Decrease and increase in the annual mean H_s among models are consistent over a considerable area of the global ocean, around 20.1% and 22.8%, respectively (splitted areas in Figure 4). Projected increases are mainly limited to the Southern Hemisphere (SH) midlatitudes and eastern Tropical Pacific. The magnitude of these changes is around 0.06–0.09 m in the Tropical Pacific while these changes are expected to achieve values higher than 0.3 m in the Southern

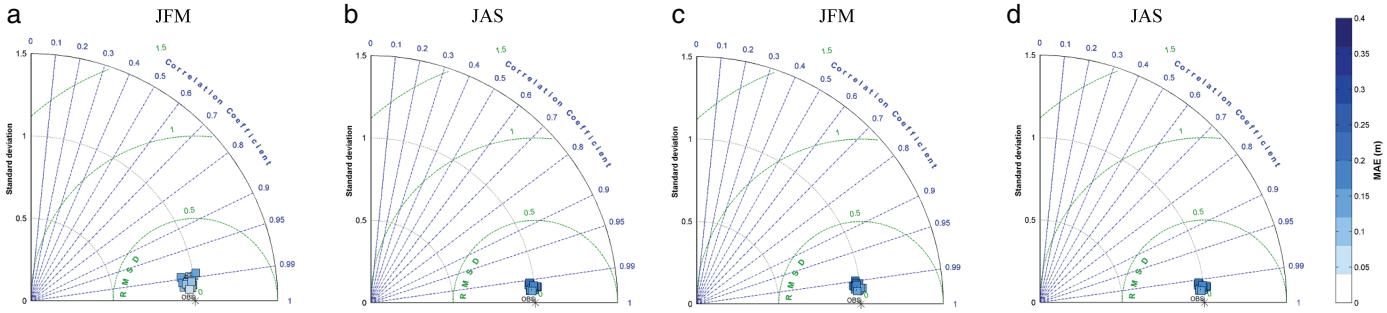

Figure 3. Taylor diagram for mean global H_s spatial patterns for JFM (a), JAS (b) and for mean global T_p spatial patterns for JFM (c), and JAS (d). Each square correspond to the projection of each GCM and the ensemble projection. The diagram shows the spatial Pearson correlation coefficient, centered root mean squared difference and standard deviation. Color inside the squares represents the spatially averaged mean absolute error (MAE).

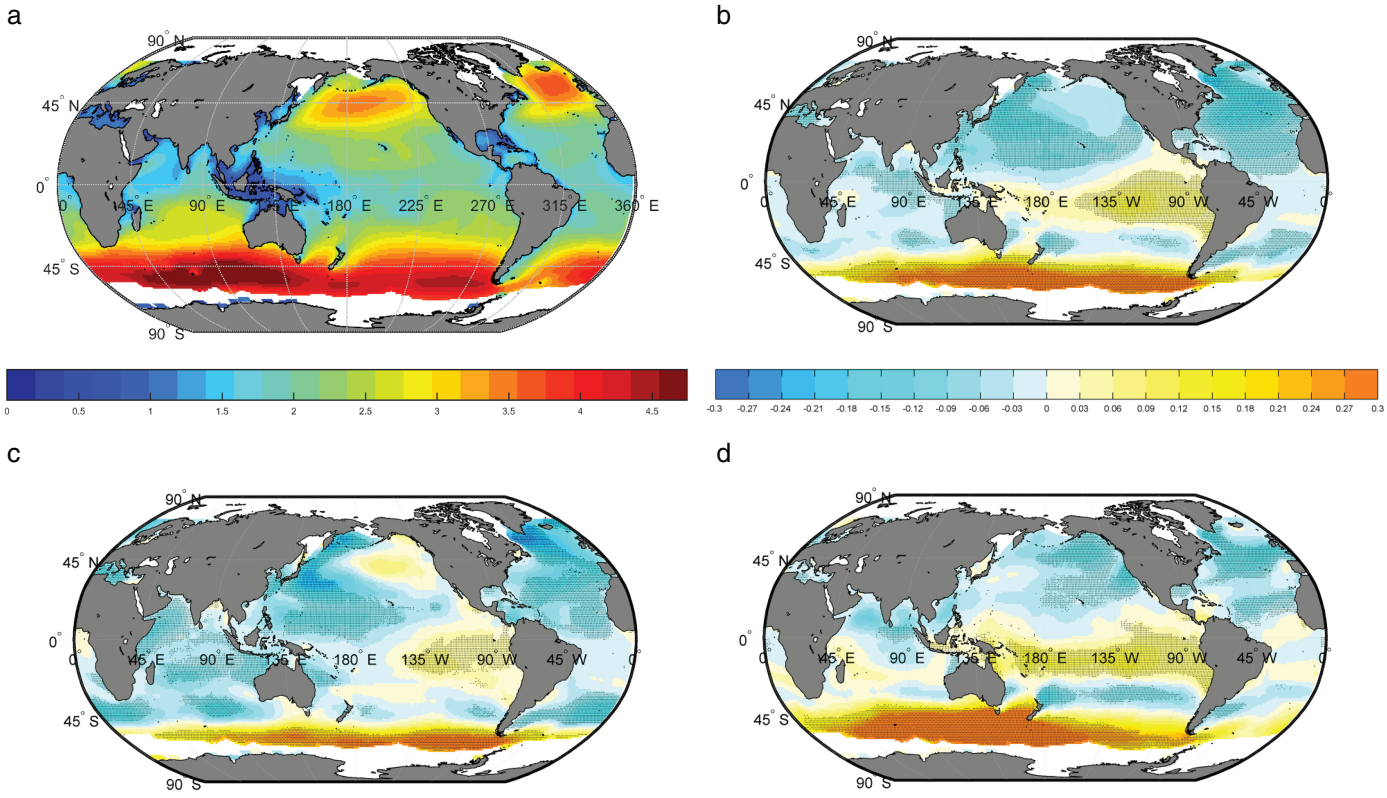

Figure 4. (a) Multimodel annual mean significant wave height (m) for the time slice 1979–2005. (b–d) Multimodel projected changes in annual, JFM, JAS mean significant wave height for future period 2070–2100 relative to present climate (1979–2005) for RCP8.5 scenario. Stippling represents areas where the magnitude of the multimodel ensemble mean exceeds the intermodel standard deviation.

Ocean (SO). Similar areas with projected increases are detected in *Hemer et al*. [2013] due to strengthening of the SO westerlies that increases swell dominance at high latitudes in the SH. Annual mean H_s decreases are projected in the midlatitudes at the North Atlantic basin, the North Pacific basin and Southern Hemisphere, that can be attributed to the poleward displacement of the extratropical storm belts [*Chang et al*., 2012]. The magnitude of these decreases are around 0.06–0.09 m. Spatial patterns of increase changes in the SO are reinforced during JAS due to the seasonal behavior of the westerlies. The area of slight significant increase of the JAS H_s is expanded to the western part of the South Tropical Pacific which is consistent with an intensification of Tropical Pacific trade winds [*De Boisséson et al*., 2014]. The magnitude of decreases is amplified in the western North Pacific and North Atlantic Ocean during JFM, reaching values almost of 0.3 m. The area of the global ocean with consistent decreases is reduced to 16.8% in JFM.

Figure 5 shows the 30-model ensemble mean projected changes in annual and seasonal (JFM, JAS) T_p for the period 2070–2100 relative to the period 1979–2005 for the RCP8.5 scenario. The area of projected T_p increases is more extensive than the area of H_s increases (36.2%) because the wave period reflects distant generated swells while H_s changes are more directly related with wind changes. The strengthening of the westerlies in the SH extra tropics involves more momentum transfer to the ocean waves that it is detected by the intensification of the T_p close to the equator. This increment is not seen in the H_s due to the balance between diminished trade winds (less energy in the short periods) and the poleward displacement of the extratropical storms in the SO (H_s attenuation by radial dispersion) which explain the apparently uncoherent spatial patterns of change in H_s and T_p. This effect is also detected along eastern coast of the Pacific Ocean as a residual signal of the swells propagating northwards from the SO. Maximum mean T_p increases are around 0.3 s in South Pacific Ocean. The increase/decrease of the boreal winter southern swell/sea component is also perceptible over the Indian Ocean as demonstrated by the increased T_p over the Arabian Sea. This difference might be caused by the weakening of the Monsoon circulation [*IPCC*, 2013], also reflected in H_s decreases, especially during boreal winter, which helps to reinforce the south swell component in the distribution of wave energy and, therefore, in the T_p. Although IPCC AR5 consistency about changes in the southwest Monsoon led to consider as robust the projected decrease [*Li et al*., 2015], there are long-standing biases of climate models limiting the skill of the projection in this part of the globe. The observed T_p decreases in the North Atlantic Ocean and most of the North Pacific, as far as the tropics, are due to the poleward displacement of the storm tracks. Maximum mean T_p decreases are around 0.3 s in the western coast of the North Pacific Ocean during winter.

Comparisons of projected changes for scenarios RCP4.5 and RCP8.5 are presented in Figure 6. This figure shows the interannual variability of the regional mean changes of the multimodel projected annual mean H_s (expressed in %) for the Southern Ocean (the area with the highest projected increases, panel a) and for the North Atlantic (where consistent decreases are expected along the whole year, panel b). The 5th, 25th,

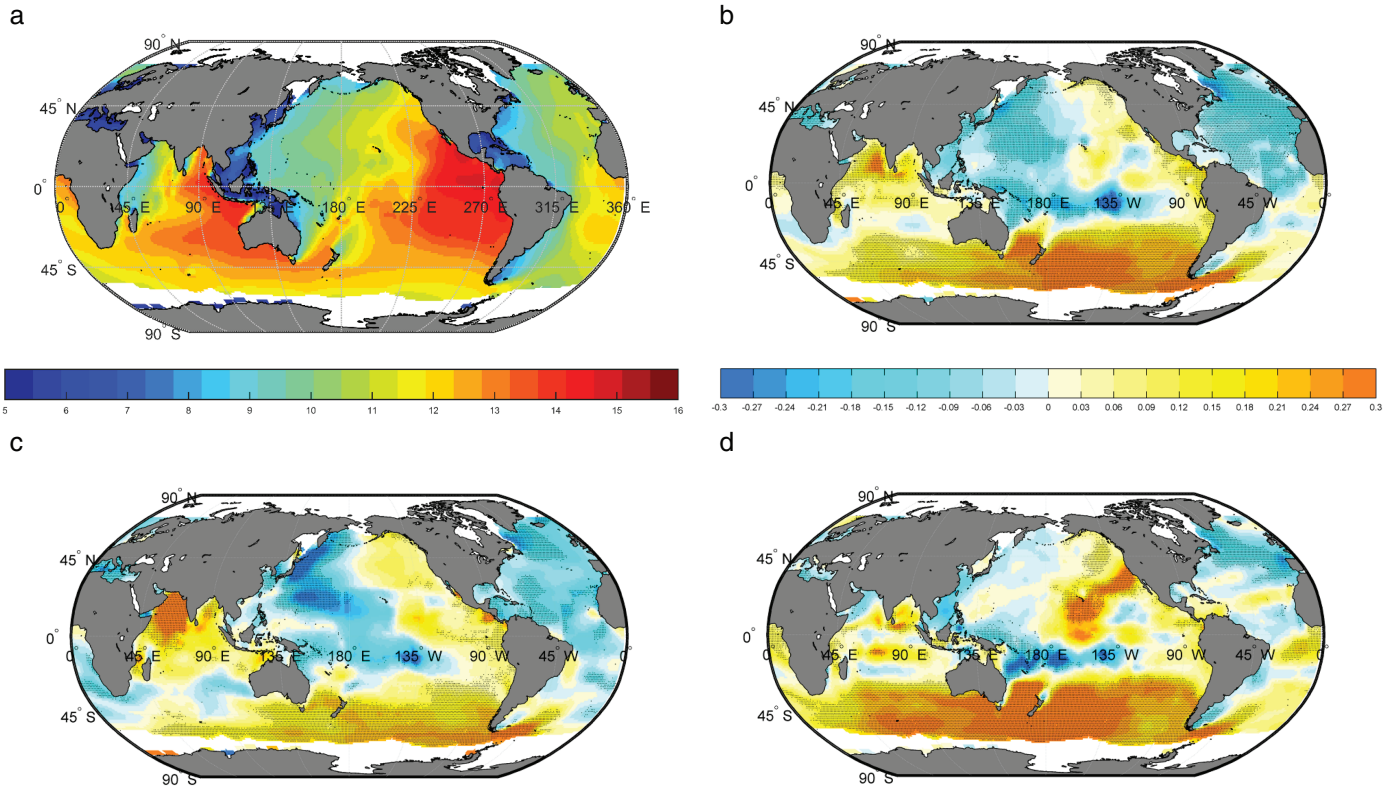

Figure 5. (a) Multimodel annual mean wave peak period (s) for the time slice 1979–2005. (b–d) Multimodel projected changes in annual, JFM, JAS mean wave period for future period 2070–2100 relative to present climate (1979–2005) for RCP8.5 scenario. Stippling represents areas where the magnitude of the multimodel ensemble mean exceeds the intermodel standard deviation.

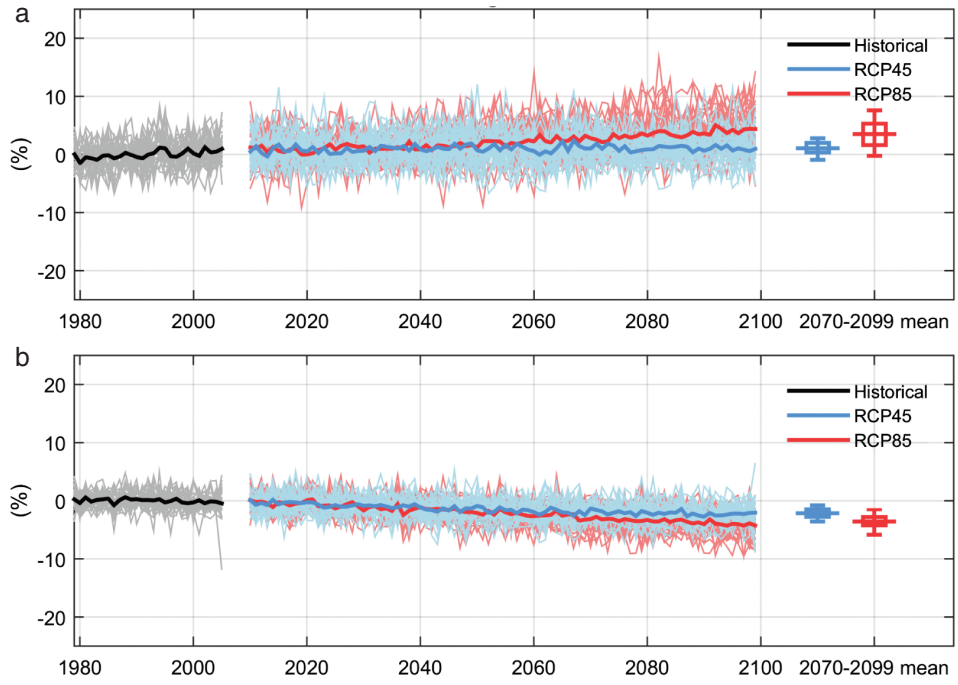

Figure 6. Time series of annual mean H_s change relative to 1979–2005 averaged subdomain ID06 (Southern Ocean, panel a) and ID09 (North Atlantic Ocean, panel b). Thin lines denote one ensemble member per model, thick lines the multimodel mean. On the right-hand side the 5th, 25th, 50th (median), 75th, and 95th percentiles of the distribution of 30-year mean changes are given for 2070–2099 in the RCP4.5 and RCP8.5 scenarios.

50th (median), 75th, and 95th percentiles of the distribution of 30-year mean changes for 2070–2099 in the RCP4.5 and RCP8.5 scenarios are shown in the right part of each panel, showing a corresponding positive or negative changes The magnitude of the changes associated with the RCP8.5 scenario is expected to be higher than with the RCP4.5. The spatial patterns of the changes in annual mean H_s and annual mean T_p for RCP4.5 are similar to the change patterns for RCP8.5 (not shown) but of smaller magnitude.

5. Regional Climate Projections

Two regions have been selected to show the applicability of the semi-supervised weather patterns obtained at global scale at 1.0°×1.0° resolution to project waves at regional scale. The coastal regions selected are Southern Australia and Western South America. These regions are considered because they are located in areas where wave height increases have been estimated. The statistical relationship is established using the GOW2 grid nodes in the continental shelf along world coastlines at a 0.25° spatial resolution as a reference database. The empirical distribution of the hourly wave parameters (H_s, T_p, θ) of each wave grid node for WTs of the closest node of the 1.0°×1.0° grid is calculated (Step 5 of the adopted statistical downscaling framework). The future empirical distribution of the wave variables is inferred for each GCM using its corresponding future WT probabilities. Changes of the mean H_s, the 95th percentile of H_s, the mean T_p and the mean θ are estimated for each GCM (Step 6 of the proposed framework). Figure 7a shows the box plots of these changes along the Southern coast of Australia. On each box, the central mark is the median, the edges of the box are the 25th and 75th percentile, the whiskers extend to the most extreme values (1.5 times the difference between the 25th percentile and the 75th percentile) and outliers are plotted individually. The global projections in this region present a positive mean H_s change from the west to the east. The regional results highlight the spatial variability in the wave magnitude with local modulations and local sheltering effects. A similar pattern of change is found in the extreme wave heights (95th percentile of H_s, H_{p95}). The intermodel variability is more noticeable in extreme wave heights and in locations where wave changes are expected to be higher. The mean T_p changes are smaller than 0.25 s at all locations, being the intermodel variability around the mean change magnitude. Regarding wave direction, a general anticlockwise change of around 2°–3° is expected in almost all positions due to a greater southerly wave component associated

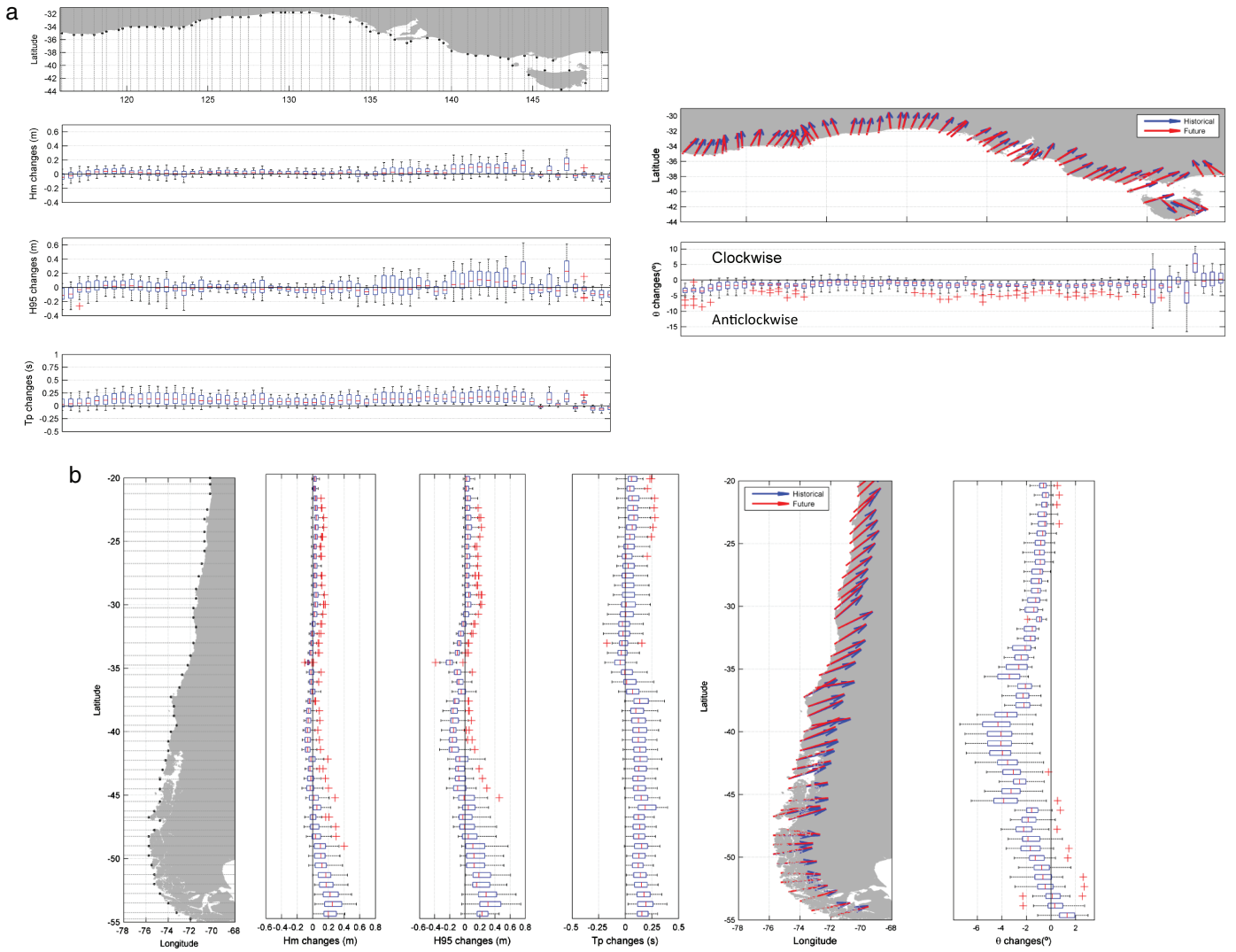

Figure 7. Regional multimodel projections (RCP8.5, 2071–2099 with respect to 1979–2005) for wave statistics along the coastline of: (a) Southern Australia (locations, intermodel changes of H_s, H_{p95}, T_p, present and future θ, intermodel changes of θ); (b) Western South America (locations, intermodel changes of H_s, H_{p95}, T_p, present and future θ, intermodel changes of θ).

with projected poleward shifts of the storm tracks [*Hemer et al*., 2013]. Figure 7b shows the boxplot of wave changes along the western coast of South America. Regional changes reflect the global pattern, an increase in the north part (0.03–0.06 m), a decrease in the middle (0.03–0.06 m) and higher increase in the south part of this region (0.2 m). Focusing the analysis of the results in this southern area with higher increases, the intermodel variability is almost of the same magnitude of mean changes. In this case, almost all the GCMs project a positive change, giving a consistent variation compared with the results at the southern Australia. Similar consistency is expected regarding T_p changes, with mean changes close to 0.25 s. Wave direction changes reach values around 4° anticlockwise near latitudes 40°–45°S, obtaining a similar change spatial variation as in *Hemer and Trenham* [2016].

6. Regional Assessment of Coastal Climate Change Impacts

The vertical component of the wave run-up is defined using a simple empirical formula which depends on significant wave height and wave period for dissipative beaches $(0.043 \times (H_s \times L_0)^{0.5}$, being L_0 the wave length in deep water, *Stockdon et al*. [2006]. Overtopping over a rubble-mound breakwater is calculated using the empirical formulation developed by Owen et al. [1980], which is function of H_s, mean sea level and breakwater freeboard. A threshold equal to 0.1 L s^{-1} m^{-1} is the tolerable overtopping mean discharge for

pedestrians, EurOtop [*Pullen et al*., 2007]. A freeboard which guarantees an operability around 95% is considered in each location. Historical time series of TWL and overtopping are calculated along the southern coast of Australia and west coast of South America taking into account the wave transformation toward the coast using wave linear theory. The statistical relationship is established between the time series of TWL or overtopping to perform a direct downscaling of the coastal impact indicators. A single predictand for these indicators solves the problem of physical consistency required among the marine drivers when they are individually downscaled. In this study, the predictor to downscale the indicators is the same as for the waves. The empirical distribution of the hourly TWL or overtopping at each coastal location associated with WTs of the closest node of 1.0°×1.0° grid is calculated (Step 5 of the proposed statistical downscaling framework). The effect of SLR is also introduced in the climate change variations of the coastal impact indicators. The effect of SLR in the TWL or overtopping is addressed differently. In the case of the TWL, the future distribution is inferred using the empirical TWL distribution associated with each WT, using the historical conditions, and the corresponding WT probabilities for each GCM, following by a simple shift of this entire future distribution toward a higher sea level (i.e., a shifted mean equal to the SLR). In the case of the overtopping, changes in the freeboard due to SLR are reflected in nonlinear changes in the discharge rates. An empirical distribution of the overtopping associated with each WT is calculated for the historical hourly wave conditions at the sea level by the end of the 21st century. The future total distribution is estimated using these empirical distributions for each WT and the corresponding future WT probabilities. Changes of the 99th percentile of TWL or the number of hours over 0.1 L s^{-1} m^{-1} discharge are estimated for each GCM (Step 6 of the proposed framework) as the difference between future and present values.

Panels a1 and b1 of Figure 8 show the 99th percentile of the TWL for the present period (1979–2005), the multiensemble indicator changes only due to changes in waves and SS for future period (2070–2100) relative to present values (1979–2005), the regional SLR by 2100 for RCP8.5 scenario and the multimodel future TWL (period 2070–2099) for RCP8.5 scenario taking into account the combination wave and storm-surge changes and SLR. Present 99th percentile of TWL along the southern coast of Australia varies from 0.6 to 1.7 m, mainly due to higher SSs at the eastern part and local tides at Northern Tasmania. Slight positive and negative changes of the 99th percentile of TWL due to atmospheric changes are expected along this coast, which represent a small percentage compared to those due to SLR (around 0.7 m). Present TWL varies between 1.3 and 1.8 m along the western coast of South America, the highest values of the 99th percentile of TWL can be found in the south region due to higher wave heights and SSs. Changes in the flooding indicator reflects mainly regional SLR, with spatial differences of 0.25 m between the northern (around 0.65 m) and southern part (around 0.40 m). The spatial variability of the future TWL is reduced, expecting a TWL around 2.1 m by the end of 2100 along the coast of this region.

Panels a2 and b2 of Figure 8 shows the hypothetical freeboard needed to ensure a harbor operability of 95%, the operability, as the exactly hours per year in which overtopping exceeds the threshold of 0.1 L s^{-1} m^{-1}, and multimodel operability changes in hours per year by the end of the 2100 for RCP8.5 scenario. The multimodel ensemble changes are calculated as the mean difference between hours exceeding the selected threshold in the future period (from the inferred future distribution of the overtopping, taking into account changes in waves and SLR) and the hours exceeding the same threshold in the present period (from the inferred present distribution based on historical overtopping) for each GCM. The freeboard along the southern coast of Australia varies from 1.0 to 17.0 m, determined by the severity of the local wave climate, which has been propagated using linear theory. The hours per year over the overtopping threshold are around 400 h (operability is around 94%–97%). An increase in the number of hours over the threshold is expected in the future period (2070–2099), being around 500 h in the west part and 200 h in the east part. Higher operability changes are usually expected in locations with smaller freeboard (western part of South Australia) because these breakwaters are more sensitive to SLR, increasing the number of overtopping events. Larger freeboards will work as a protection from a permanent SLR because its design is determined by the highest extreme waves. Although discharge rates are expected to rise in the future, the number of overtopping events does not increase significantly as in the case of breakwater with lower freeboard. Certain locations with small freeboards are not expected to suffer high operability changes. Although SLRs, the high amount of calm conditions will be maintained, expecting an increase of the magnitude

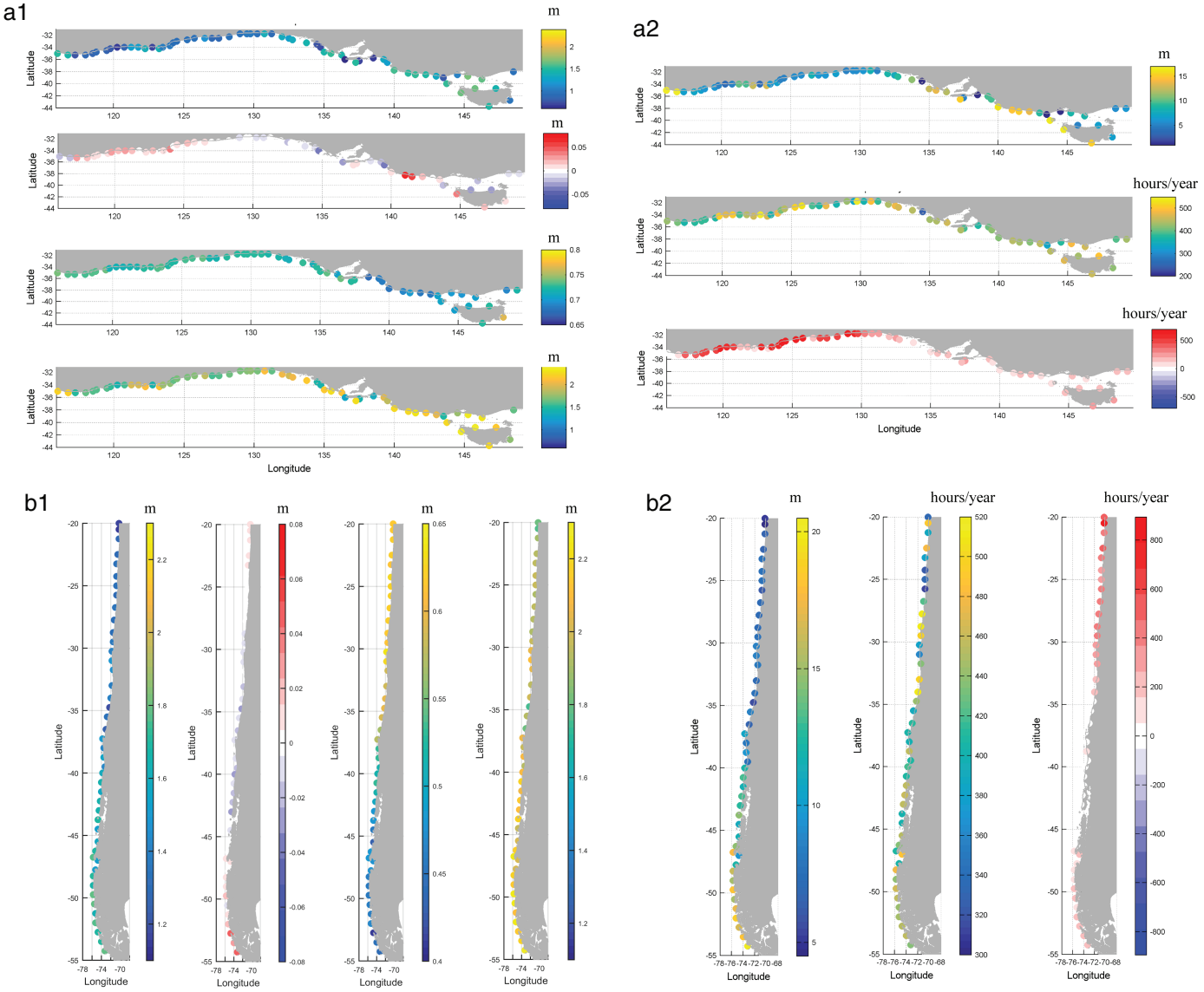

Figure 8. Regional climate change assessment of coastal impacts: (a1 and b1) the 99th percentile of the TWL for the present period (1979–2005), the multiensemble indicator changes only due to changes in waves and storm surge, the regional sea level rise [from *Slangen et al.*, 2014] by 2100 and the multimodel future TWL (period 2070–2099) taking into account wave and storm-surge changes and sea level rise for RCP8.5 scenario (a1: Southern Australia; b1: Western South America); (a2 and b2) the freeboard corresponding to an operability near 95%, the exactly hours per year overtopping exceeds the threshold of 0.1 L s^{-1} m^{-1} and multimodel operability changes in hours per year for future period (2070–2100) relative to present period (1979–2005) (a2: Southern Australia; b2: Western South America).

of overtopping but not a significant increase in the number of overtopping events. The freeboard along the west coast of South America varies from 4.5 to 20.5 m due to a more extreme wave climate in this region. The spatial pattern of the changes in operability reflects the vulnerability of breakwaters to SLR as a function of the freeboard combined with wave severity. The northern part of this region is expected to be more affected by climate change (increases of 600–800 h per year over the threshold due to lower freeboards) compared with the southern part (increases around 200 h with higher freeboards). Although wave changes are included in the future overtopping distributions, future changes of operability are mainly due to SLR.

Changes in flooding and operability are only shown for the mean multimodel ensemble. However, the intermodel uncertainty for different climate change scenarios can be easily quantified using this statistical framework.

7. Discussion and Conclusions

The objective of the proposed statistical downscaling framework is multiple: (1) to improve the performance of the global wave projections quantifying the associated uncertainty due to climate change scenarios and GCMs; (2) to make multimodel regional wave projections more feasible; and (3) to assess regional climate change coastal impacts. A weather-typing SDM is applied at global scale based on an ocean wave genesis characterization.

Regarding the results, multimodel ensemble global wave projections inform about consistent annual mean H_s increases expected in the Southern Ocean and eastern Pacific, consistent annual H_s decreases expected in the North Atlantic Ocean, western North Pacific basin, Indian Ocean and Southern Hemisphere midlatitudes. The magnitude of the increases is around four times higher than the magnitude of the decreases. Regarding T_p changes, increases are expected in the Southern Ocean, Eastern Pacific and Indian Ocean, informing about larger area of positive changes because an intensification of wave energy generation in the southern basin is reflected at further distance. T_p decreases are predicted in the North Atlantic Ocean, the Western Pacific Ocean until the Tropic of Capricorn. The results at regional scale along two coastal regions (Australia and western South America) reflect regional features in wave changes. Intermodel variability is of the same order of magnitude of the mean multimodel ensemble changes and not always with intermodel consistency. Regional coastal impact assessment is carried out downscaling directly the impact indicators: TWL and operability. Changes in the 99th percentile of TWL and changes in the number of hours per year in which overtopping is over a certain discharge threshold are calculated taking into account changes of marine variables and SLR. Changes of the 99th percentile of TWL mainly reflect the regional SLR because changes due to climate change variations of waves and SS are not of significant magnitude. Ratios of changes due to waves and SSs around 7%–16% under RCP8.5 are obtained along the coast of Europe using climate change projections of each variable independently [*Vousdoukas et al*., 2017]. Changes in port operability are also essentially caused by SLR, being breakwater with lower freeboard more sensitive to SLR.

As a summary, the advantages of the proposed statistical framework compared with DD or other SDMs are: (1) the spatial resolution of wave projections depends on the historical wave database used as reference, not fixed as in dynamical simulations (e.g., global projections at 1.0° or regional projections at 0.25° or higher). Semi-supervised WTs at a 1.0°×1.0° grid can be used to downscale wave climate at different spatial resolutions; (2) low computational effort is required to quantify uncertainty associated with climate change scenarios and various GCMs, to cover the whole century (not limited to the end of the 21st century as most dynamical simulations) and to update CMIP outputs; (3) multivariate marine projections can be obtained using the same statistical scheme (not limited to wave height as other statistical methodologies); and (4) coastal impact can be assessed by means of direct downscaling of impact indicators which integrate climate change variations of various marine hazards and SLR. Table 2 collects the main difference between DD, existing statistical downscaling (SD) and the proposed framework.

Characterization of ocean wave generation areas in 11 patterns facilitates the application of the statistical framework at a global scale. However, not all locations within the same subdomain are properly represented by the corresponding predictor, especially when waves are mainly generated by local conditions. A particularized research of the optimum predictor-domain configuration should be carried out in order to improve the performance of the statistical method. Nevertheless, the guided WT classification by local wave climate assures an acceptable level of skill of the statistical downscaling model. The main disadvantage of the methodology is that it is not able to estimate hourly future wave conditions to force process based impact models. Another limitation is that the analysis of future extreme events is restricted to changes of high percentiles inferred from the empirical distribution of the predictand (H_s, TWL, or overtopping). Although the severity of inundation is usually characterized using return periods, the regional assessment of coastal flooding by means of the 99th percentile of TWL provides an overarching impact of climate change due to changes in the storminess and SLR. Regarding port operability, the impact is quantified as the changes in the number of hours overtopping exceeds a threshold corresponding to a percentile around the 95th. Future work will be focused on improving the proposed methodology based on WTs to develop a weather generator of hourly marine conditions which models the temporal and inter-variable dependence.

Acknowledgments
The authors acknowledge the support of the Spanish Ministerio de Economía y Competitividad (MINECO) and European Regional Development Fund (FEDER) under Grant BIA2015-70644-R (MINECO/FEDER, UE). The authors are grateful to Nicolás Ripoll for his help in the performing the statistical simulations. The DAC data is produced by CLS Space Oceanography Division and distributed by Aviso, with support from Cnes (http://www.aviso.altimetry.fr/). The CMIP5 sea level pressure data are available at http://cmip-pcmdi.llnl.gov/cmip5/data_portal.html. Mean sea level projections are available at ftp://ftp.icdc.zmaw.de/ar5_sea_level_rise/.

Table 2. Properties of Dynamical Downscaling (DD), Existing Statistical Downscaling (SD) and the Proposed Framework

Properties	DD	SD	Proposed Framework
Spatial resolution	Around 1.0° at a global scale Around 0.25°/0.125° (enclosed seas) at regional scale	Around 1.0° at a global scale Around 0.125° at regional scale	Depends on the underlying wave hindcast database In this work: Global: 1.0°, Regional: 0.25°
Time resolution	Hourly	Hourly Monthly	Monthly
Extreme changes	Return periods from hourly projections	Return periods from hourly projections	High percentiles from future distribution
Temporal coverage	Usually end of 21st century	21st century	21st century
Parameter dimensionality	Multivariate	Univariate (H_s)	Multivariate
Uncertainty due to climate change scenarios and GCMs	1 or 2 RCPs Subset of GCMs (max. 8)	2 RCPs 20 GCMs (CMIP5)	2 RCPs 30 GCMs (CMIP5)
Update computational effort	Very high	Low	Very low
Influence of predictand quality	Independent	Dependent	Dependent
Impact assessment	A percentage of change from global scale From regional projections with a correction of the climate bias	Coastal impacts which only depends on H_s	Direct downscaling of impact indicators at spatial scale available

References

Arns, A., S. Dangendorf, J. Jensen, S. Talke, J. Bender, and C. Pattiaratchi (2017), Sea-level rise induced amplification of coastal protection design heights, *Sci. Rep.*, *7*, art. no. 40171. https://doi.org/10.1038/srep40171.

Brown, S., R. J. Nicholls, J. A. Lowe, and J. Hinkel (2016), Spatial variations of sea-level rise and impacts: An application of DIVA, *Clim. Change*, *134*(3), 403–416. https://doi.org/10.1007/s10584-013-0925-y.

Camus, P., M. Menéndez, F. J. Méndez, C. Izaguirre, A. Espejo, V. Cánovas, J. Pérez, A. Rueda, I. J. Losada, and R. Medina (2014), A weather-type statistical downscaling framework for ocean wave climate, *J. Geophys. Res.: Oceans*, *119*, 2014. https://doi.org/10.1002/2014JC010141.

Camus, P., A. Rueda, F. J. Méndez, and I. J. Losada (2016), An atmospheric-to-marine synoptic classification for statistical downscaling marine climate, *Ocean Dyn*. https://doi.org/10.1007/s10236-016-1004-5.

Cannon, A. J. (2012), Regression-guided clustering: A semisupervised method for circulation-to-environment synoptic classification, *J. Appl. Meteorol. Climatol.*, *51*, 185–190. https://doi.org/10.1175/jamc-d-11-0155.1.

Carrère, L., and F. Lyard (2003), Modeling the barotropic response of the global ocean to atmospheric wind and pressure forcing - comparisons with observations, *Geophys. Res. Lett.*, *30*. https://doi.org/10.1029/2002GL016473.

Casanueva, A., M. D. Frías, S. Herrera, D. San-Martín, K. Zaninovic, and J. M. Gutiérrez (2014), Statistical downscaling of climate impact indices: Testing the direct approach, *Clim. Change*, *127*(3–4), 547–560. https://doi.org/10.1007/s10584-014-1270-5.

Casanueva, A., S. Herrera, J. Fernández, and J. M. Gutiérrez (2016), Towards a fair comparison of statistical and dynamical downscaling in the framework of the EURO-CORDEX initiative, *Clim. Change*, *137*(3–4), 411–426. https://doi.org/10.1007/s10584-016-1683-4.

Casas-Prat, M., X. L. Wang, and J. P. Sierra (2014), A physical-based statistical method for modeling ocean wave heights, *Ocean Model.*, *73*, 59–75. https://doi.org/10.1016/j.ocemod.2013.10.008.

Chang, E. K. M., Y. Guo, and X. Xia (2012), CMIP5 multimodel ensemble projection of storm track change under global warming, *J. Geophys. Res.*, *117*, D23118. https://doi.org/10.1029/2012JD018578.

De Boisséson, E., M. A. Balmaseda, S. Abdalla, E. Källén, and P. A. E. M. Janssen (2014), How robust is the recent strengthening of the Tropical Pacific trade winds? *Geophys. Res. Lett.*, *41*(12), 4398–4405. https://doi.org/10.1002/2014GL060257.

Dobrynin, M., J. Murawsky, and S. Yang (2012), Evolution of the global wind wave climate in CMIP5 experiments, *Geophys. Res. Lett.*, *39*, L18606. https://doi.org/10.1029/2012GL052843.

Erikson, L. H., C. A. Hegermiller, P. L. Barnard, P. Ruggiero, and M. vanOrmondt (2015), Projected wave conditions in the Eastern North Pacific under the influence of two CMIP5 climate scenarios, *Ocean Model.*, *96*, 171–185. https://doi.org/10.1016/j.ocemod.2015.07.004.

Hallegatte, S., C. Green, R. J. Nicholls, and J. Corfee-Morlot (2013), Future flood losses in major coastal cities, *Nat. Clim. Change*, *3*(9), 802–806. https://doi.org/10.1038/nclimate1979.

Hallegatte, S., and K. J. Mach (2016), Make climate-change assessments more relevant, *Nature*, *534*(7609), 613–615. https://doi.org/10.1038/534613a.

Hallegatte, S., N. Ranger, O. Mestre, P. Dumas, J. Corfee-Morlot, C. Herweijer, and R. M. Wood (2011), Assessing climate change impacts, sea level rise and storm surge risk in port cities: A case study on Copenhagen, *Clim. Change*, *104*(1), 113–137. https://doi.org/10.1007/s10584-010-9978-3.

Hemer, M. A., Y. Fan, N. Mori, A. Semedo, and X. L. Wang (2013), Projected changes in wave climate from a multi-model ensemble, *Nat. Clim. Change*, *3*, 471–476. https://doi.org/10.1038/nclimate1791.

Hemer, M. A., and C. E. Trenham (2016), Evaluation of a CMIP5 derived dynamical global wind wave climate model ensemble, *Ocean Model.*, *103*, 190–203. https://doi.org/10.1016/j.ocemod.2015.10.009.

Hinkel, J., D. Lincke, and A. T. Vafeidis (2014), Coastal flood damage and adaptation costs under 21st century sea-level rise, *Proc. Natl. Acad. Sci. USA*, *11*(9), 3292–3297. https://doi.org/10.1073/pnas.1222469111.

IPCC (2013), Climate change 2013: The physical science basis, in *Contribution of Working Group I to the Fifth Assessment Report of the Intergovernmental Panel on Climate Change*, edited by T. F. Stocker, D. Qin, G.-K. Plattner, M. Tignor, S. K. Allen, J. Boschung, A. Nauels, Y. Xia, V. Bex and P. M. Midgley, Intergovern. Panel Clim. Change, Geneva.

Le Cozannet, G., M. Garcin, M. Yates, D. Idier, and B. Meyssignac (2014), Approaches to evaluate the recent impacts of sea-level rise on shoreline changes, *Earth Sci. Rev.*, *138*, 47–60. https://doi.org/10.1016/j.earscirev.2014.08.005.

Li, G., S.-P. Xie, and Y. Du (2015), Monsoon-induced biases of climate models over the tropical Indian Ocean, *J. Clim.*, *28*(8), 3058–3072. https://doi.org/10.1175/jcli-d-14-00740.1.

Martínez-Asensio, A., M. Marcos, M. N. Tsimplis, G. Jordà, X. Feng, and D. Gomis (2016), On the ability of statistical wind-wave models to capture the variability and long-term trends of the North Atlantic winter wave climate, *Ocean Model.*. https://doi.org/10.1016/j.ocemod.2016.02.006.

Mentaschi, L., M. I. Vousdoukas, E. Voukouvalas, A. Dosio, and L. Feyen (2017), Global changes of extreme coastal wave energy fluxes triggered by intensified teleconnection patterns, *Geophys. Res. Lett.*, *44*(5), 2416–2426.

Mori, N., T. Shimura, T. Yasudaa, and H. Masea (2013), Multi-model climate projections of ocean surface variables under different climate scenarios–future changes of waves, sea level and wind, *Ocean Eng.*, *71*, 122–129. https://doi.org/10.1016/j.oceaneng.2013.02.016.

Mori, N., T. Yasuda, H. Mase, T. Tom, and Y. Oku (2010), Projection of extreme wave climate change under global warming, *Hydrol. Res. Lett.*, *4*, 15–19. https://doi.org/10.3178/hrl.4.15.

Nicholls, R. J., N. Marinova, J. A. Lowe, S. Brown, P. Vellinga, D. De Gusmão, J. Hinkel, and R. S. J. Tol (2011), Sea-level rise and its possible impacts given a 'beyond 4 °C world' in the twenty-first century, Philosophical Transactions of the Royal Society A: Mathematical, *Phys. Eng. Sci.*, *369*(1934), 161–181. https://doi.org/10.1098/rsta.2010.0291.

Owen, M.W. (1980), Design of seawalls allowing for wave overtopping, *Rep. EX924*, Hydraulics Research Wallingford, U. K.

Perez, J., M. Menendez, P. Camus, F. J. Mendez, and I. J. Losada (2015), Statistical multi-model climate projections of surface ocean waves in Europe, *Ocean Model.*, *96*, 161–170. https://doi.org/10.1016/j.ocemod.2015.06.001.

Perez, J., M. Menendez, and I. J. Losada (2017), GOW2: A global wave hindcast for coastal applications, *Coastal Eng.*, *124*, 1–11. https://doi.org/10.1016/j.coastaleng.2017.03.005.

Perez, J., M. Menéndez, F. J. Méndez, and I. J. Losada (2014), ESTELA: A method for evaluating the source and travel-time of the wave energy reaching a local area, *Ocean Dyn.* https://doi.org/10.1007/s10236-014-0740-7.

Pullen, T., N. W. H. Allsop, T. Bruce, A. Kortenhaus, H. Schüttrumpf, and J. W. van derMeer (2007), EurOtop—Wave overtopping of sea defences and related structures: Assessment manual, *Die Küste*, *73*, 193.

Ranasinghe, R. (2016), Assessing climate change impacts on open sandy coasts: A review, *Earth Sci. Rev.*, *160*, 320–332. https://doi.org/10.1016/j.earscirev.2016.07.011.

Rueda, A., S. Vitousek, P. Camus, A. Tomás, A. Espejo, I. J. Losada, P. Barnard, L. Erikson, P. Ruggiero, B. G. Reguero, et al. (2017), A global classification of coastal flood hazard climates associated with large-scale oceanographic forcing, *Sci. Rep.*. https://doi.org/10.1038/s41598-017-05090-w.

Saha, S., S. Moorthi, X. Wu, J. Wang, S. Nadiga, P. Tripp, D. Behringer, Y. T. Hou, H. Y. Chuang, M. Iredell, et al. (2014), The NCEP climate forecast system version 2, *J. Clim.*, *27*, 2185–2208. https://doi.org/10.1175/jcli-d-12-00823.1.

Semedo, A., R. Weisse, A. Behrens, A. Sterl, L. Bengtsson, and H. Günther (2013), Projection of global wave climate change toward the end of the twenty-first century, *J. Clim.*, *26*(21), 8269–8288. https://doi.org/10.1175/jcli-d-12-00658.1.

Shimura, T., N. Mori, and H. Mase (2015), Future projection of ocean wave climate: Analysis of SST impacts on wave climate changes in the Western North Pacific, *J. Clim.*, *28*(8), 3171–3190. https://doi.org/10.1175/jcli-d-14-00187.1.

Sierra, J. P., and M. Casas-Prat (2014), Analysis of potential impacts on coastal areas due to changes in wave conditions, *Clim. Change*, *124*(4), 861–876. https://doi.org/10.1007/s10584-014-1120-5.

Sierra, J. P., M. Casas-Prat, M. Virgili, C. Mösso, and A. Sánchez-Arcilla (2015), Impacts on wave-driven harbour agitation due to climate change in Catalan ports, *Nat. Hazards Earth Syst. Sci.*, *15*(8), 1695–1709. https://doi.org/10.5194/nhess-15-1695-2015.

Slangen, A. B. A., M. Carson, and C. A. Katsman (2014), Modelling twenty-first century regional sea-level changes, *Clim. Change*. https://doi.org/10.1007/s10584-014-1080-9.

Stockdon, H. F., R. A. Holman, P. A. Howd, and A. H. Sallenger (2006), Empirical parameterization of setup, swash, and runup, *Coast. Eng.*, *53*, 573–588. https://doi.org/10.1016/j.coastaleng.2005.12.005.

Taylor, K. E. (2001), Summarizing multiple aspects of model performance in a single diagram, *J. Geophys. Res.*, *106*(D7), 7183–7192. https://doi.org/10.1029/2000JD900719.

Tolman, H. and the WaveWatch III® Development Group (2014), User Manual and System Documentation of WAVEWATCH III® version 4.18. *Tech. Note 316*, NOAA/NWS/NCEP/MMAB, 282 pp. +Appendices. https://doi.org/10.1021/ic501637m.

Vousdoukas, M. I., L. Mentaschi, E. Voukouvalas, M. Verlaan, and L. Feyen (2017), Extreme sea levels on the rise along Europe's coasts, *Earth's Future*, *5*(3), 304–323. https://doi.org/10.1002/2016EF000505.

Wang, C., L. Zhang, S.-K. Lee, L. Wu, and C. R. Mechoso (2014a), A global perspective on CMIP5 climate model biases, *Nat. Clim. Change*, *4*(3), 201–205. https://doi.org/10.1038/nclimate2118.

Wang, X. L., Y. Feng, and V. R. Swail (2014b), Changes in global ocean wave heights as projected using multi model CMIP5 simulations, *Geophys. Res. Lett.*, *41*(3), 1026–1034. https://doi.org/10.1002/2013GL058650.